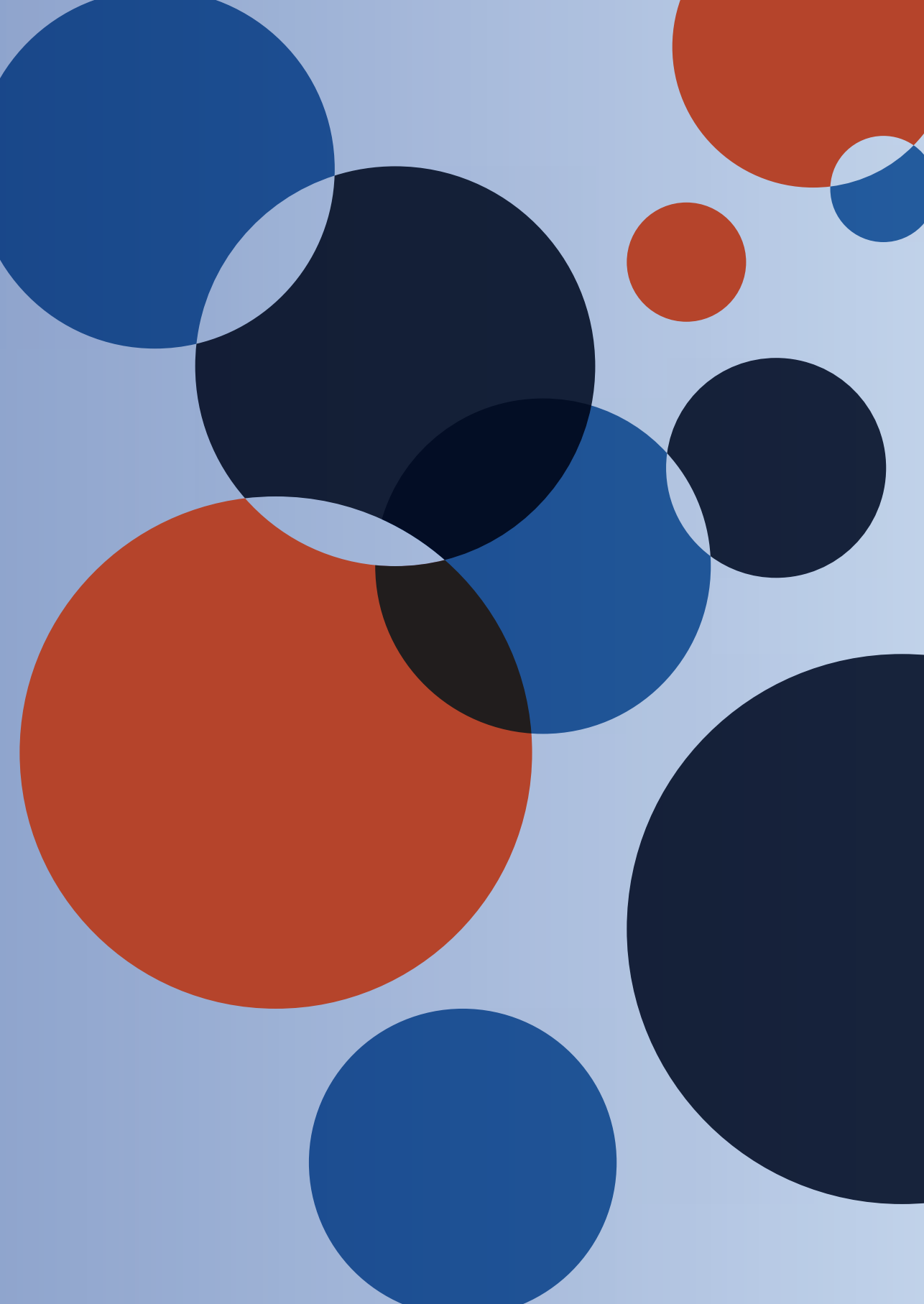

CHARACTERIZATION OF HEMOSTASIS IN MICE LACKING THE NOVEL THROMBOSIS SUSCEPTIBILITY GENE *SLC44A2*

Julia Tilburg*, Raymond Adili*, Thankam S. Nair, Megan E. Hawley, David C. Tuk, Madeline Jackson, Henri M. Spronk, Henri H. Versteeg, Thomas E. Carey, Bart J.M. van Vlijmen, Chrissta X. Maracle**, Michael Holinstat**

* / **: These authors contributed equally

Thromb Res. 2018 Nov;171:155-159.

2

Abstract

Introduction

Recent genome wide association studies (GWAS) identified a novel susceptibility locus for thrombosis, harbouring the *SLC44A2* gene which encodes the Solute Carrier Family 44 Member 2 protein (SLC44A2). Thus far, SLC44A2 has not been studied in the context of thrombosis and may be a unique contributor to thrombotic disease. Here we utilize mice lacking SLC44A2 (*Slc44a2-/-*) to evaluate a possible role of SLC44A2 in hemostasis.

Methods

Slc44a2-/- mice were evaluated in key aspects of normal hemostasis including a challenge of vascular damage by applying laser induced injury to the cremaster muscle arteriole.

Results

Slc44a2-/- mice had comparable levels of thrombin generation and gene expression of coagulation related genes, as compared to littermate wild type controls. Lower levels of circulating plasma von Willebrand factor (VWF) were measured in *Slc44a2-/-* mice, while no difference in VWF multimerization or vascular localization was detected. Upon *in vivo* laser injury of the cremaster arterioles, we detected an impairment of clot formation for *Slc44a2-/-* mice.

Conclusions

Although mice lacking SLC44A2 are normal for several hemostasis parameters, we do observe a reduction of plasma VWF levels and an altered response upon vascular damage, which suggests that SLC44A2 contributes to hemostasis upon injury. These findings are in line with the reported GWAS data and support further research on SLC44A2 in thrombosis.

Introduction

Thrombosis is a major contributor to the global health burden, with genetic predisposition being an important underlying element (1). Recently, a genome wide association study (GWAS) aimed at identifying novel genetic risk factors for venous thromboembolism (VTE, i.e. deep vein thrombosis (DVT) and pulmonary embolism (PE)), identified a susceptibility locus containing *SLC44A2* (2). Interestingly, unlike the loci previously known to associate with VTE (*ABO, F2, F5, F11, FGG, and PROCR*), the *SLC44A2* locus did not associate with hemostasis phenotypes included in the GWAS, such as enhanced thrombin generation, platelet counts and von Willebrand factor (VWF) levels (2). Moreover, a second, independent GWAS detected an association between *SLC44A2* and self-reported blood clotting events (DVT, PE, ischemic stroke), strengthening the implication that *SLC44A2* is linked to thrombosis (3). Therefore, it is plausible that SLC44A2 plays a role in the pathophysiology of thrombosis.

SLC44A2 encodes Solute Carrier Family 44 Member 2 (SLC44A2) (4), a presumed choline transporter based on its homology to other transport proteins (5). Notably, an SLC44A2 polymorphic site forms the human neutrophil antigen 3, an epitope for alloantibodies that mediate transfusion related acute lung injury (TRALI) (6, 7). TRALI, like thrombosis, has a central role in its pathogenesis for endothelial cells and neutrophils, both of which express SLC44A2, in addition to several other tissues (4). Furthermore, a recent TRALI study described SLC44A2 to be a binding partner of VWF, a key molecule in hemostasis (8). Additionally, SLC44A2 has been associated with autoimmune hearing loss, due to its importance in hair cell viability (9).

As the GWAS show an association between SLC44A2 and thrombosis, but not a mechanistic insight, further investigation of SLC44A2 with respect to its role in thrombosis is warranted. Here we utilize mice lacking SLC44A2 (*Slc442-/-*) to gain insight into the role of SLC44A2, if any, in hemostasis as a precursor to further thrombosis studies. To this end we characterized *Slc44a2-/-* mice for several parameters of hemostasis under normal conditions including a challenge of vascular injury.

Material and Methods

Slc44a2-/- mice were previously generated from mice with *Slc44a2* exons 3-10 flanked with LoxP sites (*Slc44a2fl/fl* mice) and deleter EIIa-Cre transgenic mice (9, 10). The resulting *Slc44a2-/-* mice were subsequently backcrossed to FVB/NJ (FVB) (7 generations) to form a FVB line at University of Michigan, USA. FVB*;Slc44a2+/-* mice were used to generate *Slc44a2-/-* mice used for experiments, and *Slc44a2*+/+ littermates were used as controls. At Leiden University Medical Center (LUMC), In the Netherlands, a colony of *Slc44a2-/-* mice on an C57BL/6J (B6) background was established starting from frozen B6;129Sv-*Slc44a2*$^{fl/+F2\text{-}N2}$ embryos obtained from the University of Michigan. After cryorecovery, genotyping (9) and backcross with B6 mice (Charles River, The Netherlands), *Slc44a2*fl/+ mice were again

combined with in house B6;EIIa-Cre transgenic mice ((10), originally obtained from Jackson Laboratories, Bar Harbor, USA). The resulting EIIa-Cre positive *Slc44a2*+/- mice were used to generate the *Slc44a2-/-* and control *Slc44a2*+/+ littermates (backcrossed total 5 generations to B6). Mice of both sexes were used unless indicated otherwise. Apart from previously described age related (>6 months of age) progressive hearing impairment in FVB;*Slc44a2*$^{-/-}$, no other abnormalities in *Slc44a2-/-* mice were reported (9). All experimental procedures were approved by local institutional animal welfare committees.

Sodium-citrated blood was collected directly from inferior caval vein of mice anesthetized by intraperitoneal injection of ketamine/xylazine (100 mg/kg). Plasma thrombin generation assays were performed using 10 or 20µg/mL ellagic acid (Sigma, USA) or 1pM tissue factor (Stago BNL, The Netherlands) (11). Coagulation gene profiling of lung and liver were determined by quantitative polymerase chain reaction (12). Primers are listed in Table S1. Lung and liver fibrin deposition are determined by immunoblotting with 59D8 antibody (13).

Plasma VWF levels were determined by ELISA and multimerization by immunoblot with anti-human VWF (DAKO A082, USA) as described (14), except 10-fold higher plasma concentration was used compared to VWF ELISA using human plasma. 4µM cryosections of hind leg muscle (including femoral vein and artery) and left lung lobule, immunostained for VWF (DAKO A082, USA), were imaged by confocal microscopy (Leica SP8, Germany) at 63x magnification.

Blood cell counts were assessed by Hemavet (Hemavet950FS, USA) or Sysmex (SysmexXT-2000iV, Sysmex Europe GMBH, Germany). For platelet analysis, citrated blood was drawn via orbital sinus puncture of anesthetized mice. Pooled washed platelets were obtained from blood as described before (15). The presence of SLC44A2 protein in platelets was determined by immunoblot with anti-SLC44A2 antibody as previously described (9). Platelet count was adjusted to $2.4x10^8$ platelets/mL and thrombin (0.1, 0.25, 0.5, 1.0 nM) induced platelet aggregation was measured as described before (15).

The *in vivo* response to vascular injury in mice was evaluated using a cremaster muscle arteriole injury model as described (15). Briefly, adult mice were anesthetized by intraperitoneal injection of ketamine/xylazine (100 mg/kg) and the cremaster muscle was prepared. DyLight 488-conjugated anti-GP1bβ antibody and Alexa Fluor 647-conjugated anti-fibrin antibody were administered prior to vascular injury via the jugular vein. Multiple independent injuries were induced in the arterioles of the cremaster muscle in each mouse by a laser ablation system. The dynamic accumulation of platelets and fibrin was monitored in real-time using a fluorescent microscope (Zeiss Axio Examiner Z1 fluorescent microscope with a ×63 objective and a high-speed sCMOS camera) and the data was analysed as previously described (15-18). Injury experiments for both FVB and B6 background mice were performed and analysed by one operator in a blinded fashion at the University of Michigan.

Results and Discussion

Mice deficient for SLC44A2 were originally generated for studies characterizing the role of SLC44A2 in autoimmune hearing loss and required FVB as the strain background (9). Here, we use these FVB;*Slc44a2-/-* mice and their wild type (*Slc44a2*+/+) littermates to further characterize the mice with regards to hemostasis under normal and challenging conditions (Figure 1). Additionally, elements of this characterization were repeated for *Slc44a2-/-* mice and their wild type (*Slc44a2*+/+) littermates present on a B6 background (Figure S1), as this is the preferred background in cardiovascular research.

Thrombin generation, induced both by tissue factor and ellagic acid, was unaltered in *Slc44a2-/-* mice as compared to *Slc44a2*+/+ littermate controls (Figure 1A/S1A). Changes in coagulation were also examined through transcriptional profiling of lung and liver genes (Figure 1B/1SB). As expected, *Slc44a2* was not detectable in *Slc44a2-/-* mice, confirming the genotype. Additionally, we did not observe a compensatory effect within the gene family in either line, as transcript levels of *Slc44a* family members (*Slc44a1, Slc44a3* and *Slc44a4)* remained unchanged (Figure S2), with *Slc44a5* being undetectable. In FVB *Slc44a2-/-* mice, a 12% increase in lung transcript of tissue plasminogen activator (*Plat*) was detected (p=0.018), when compared to *Slc44a2*+/+ littermates, whereas the levels remained comparable between B6 mice. Additionally, in the lung, transcript levels of *F3*, *Vwf*, *F2r*, *F8*, *Thbd*, *Tfpi* and *Serpine1* were not different and no variation in *Fga*, *F2*, *F5*, *F11* or *Proc* expression in the liver was found in either background. Furthermore, there was no detectable fibrin deposition (<2µg/mg tissue) in these tissues (Figure S3) of either background. These findings indicate that *Slc44a2-/-* mice do not display abnormalities in general coagulation, which is in line with the reported GWAS linking *SLC44A2* to VTE, but not to coagulation parameters (2).

As it was previously described that HEK293 cells overexpressing SLC44A2 bind VWF *in vitro,* we sought to determine whether VWF could be altered in *Slc44a2-/-* mice (8). In the FVB line, a non-significant 27% decrease in median plasma levels of VWF was observed in *Slc44a2-/-* mice (p=0.1996) (Figure 1C). In B6 *Slc44a2-/-* mice, median VWF plasma levels were significantly reduced by 20% (p=0.0442) (Figure S1C). SLC44A2 status did not affect VWF multimerization (Figure 1D/S1D). To visualize possible changes in VWF localization, femoral veins and arteries as well as microvessels of the lung, were stained for VWF (Figure 1E/S3/S4/S5). Although intensity of VWF was variable, we did not observe any differences in localization on the luminal side of the endothelial lining of the vessel walls nor in the microvasculature of the lung. Together these data suggest that VWF is lowered in the plasma of *Slc44a2-/-* mice, whereas multimerization and localization is unaltered.

Prior RNA-sequencing data confirmed that SLC44A2 is expressed by human platelets (19), and here we demonstrate that it is also present on murine platelets (Figure 1F). Moreover, loss of SLC44A2 does not impact platelet counts, nor amounts of other blood cells (Figure 1F/Table S2). To determine if SLC44A2 influences platelet function, we measured *ex vivo* platelet

aggregation induced both by thrombin (Figure 1G) and collagen (Figure S6), and although a trend towards accelerated thrombin induced platelet aggregation in *Slc44a2-/-* mice was visible, no significant differences between genotypes were observed.

To determine whether *Slc44a2* status could affect clot formation *in vivo*, platelet and fibrin accumulation was measured upon laser-induced injury of the cremaster arteriole using intravital microscopy (Figure 1H). Compared to control mice, clots grew to similar size in *Slc44a2-/-* mice on FVB background; however, clots in *Slc44a2-/-* mice were visually more unstable. There was no significant difference found in dynamics of platelet accumulation, although fibrin accumulation was significantly impaired in *Slc44a2-/-* mice ($p<0.0001$), which may be responsible for clot instability (Figure 1I). Interestingly, the response following laser injury in *Slc44a2-/-* mice on B6 background was also impaired with platelet accumulation significantly decreased as compared to control mice ($p<0.05$) (Figure S1E). Although the background of the mice was different, the impairment of clot formation seemed consistent across backgrounds.

We conclude that mice deficient for SLC44A2 are normal for the several hemostasis parameters that we evaluated; apart from the elevated lung *Plat* transcripts observed for Slc44a2-/- mice with an FVB background, and the reduced levels of circulating plasma VWF. Of note, a lower amount of plasma VWF was again observed for a third independent group of Slc44a2-/- mice (B6 background, -17% as compared to littermate controls, n=12, $p=0.0211$), highlighting that this observation is reproducible. Since SLC44A2 was reported to interact with VWF *in vitro*, at least in the context of TRALI (7), the observed modest lowering of plasma VWF upon SLC44A2 deficiency warrants further investigation, including VWF dependent models of thrombosis. Of note the cremaster laser injury model clot formation was previously shown to be independent of plasma VWF levels (20). Regardless, this observation, in addition to the recorded impact of SLC44A2 deficiency upon vascular challenge, suggests that SLC44A2 contributes to hemostasis in response to injury, however, whether this effect is direct or indirect remains to be determined. Nonetheless, these findings are in line with the reported GWAS (2, 3) and encourage further investigation of the role of SLC44A2 under pathological conditions i.e. thrombosis and, if any, the underlying mechanism.

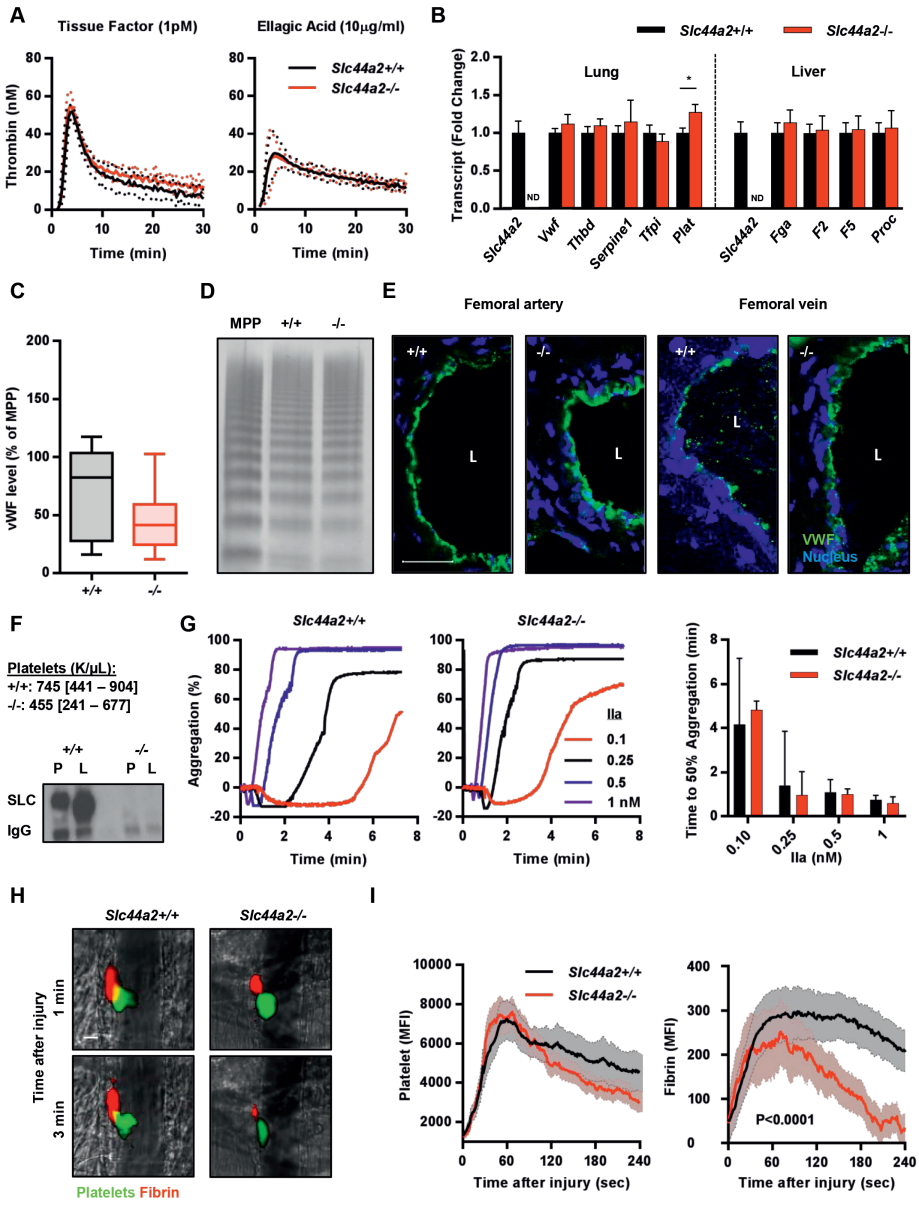

Figure 1. Characterization of hemostasis in *Slc44a2* deficient mice on an FVB background: (A) Thrombin generation in plasma from mice induced either by 1pM Tissue Factor (n=7 both groups) or 10 µg/mL ellagic acid (n=4 *Slc44a2*+/+; n=7 *Slc44a2-/-*). Solid lines represent the mean value and dotted lines the standard deviation (SD). **(B)** Gene transcript levels of *Slc44a2* and coagulation related genes in lung (n=11 *Slc44a2*+/+; n=7 *Slc44a2-/-*) and liver (n=7 both groups). The comparative threshold cycle method with β-actin as internal control was used for quantification and normalization. The mean is represented as fold change compared to *Slc44a2*+/+mice. Error bars represent the difference between

2 POWER of upper range of the mean ΔΔCt. ND; non detectable. **(C)** Level of plasma vWF expressed as a percentage (%) of the wild type controls; represented as Tukey whisker plot. **(D)** Immunoblot of VWF multimerization in plasma of *Slc44a2*+/+and *Slc44a2-/-* mice (n=7). **(E)** Confocal microscopic images of vWF (green) in femoral vein and artery. (Images representative of 5 mice per group; scale bar 30µm). L: Luminal side. **(F)** Top: Total platelet counts of *Slc44a2*+/+and *Slc44a2-/-* mice quantified as the median with range (n=5, female). Bottom: Immunoblot of *SLC44A2* (SLC) protein expression in pooled platelets (P) (n=3) and lung tissues (L) from *Slc44a2*+/+and *Slc44a2-/-* mice compared to control immunoglobulinG (IgG). **(G)** Thrombin (IIa) induced platelet aggregation using pooled platelets from *Slc44a2*+/+(left graph) and *Slc44a2-/-* (middle graph) mice. Concentrations of thrombin indicated in red (0.1nM), black (0.25nM), blue (0.5nM) and purple (1.0nM) (Representative of n=3 platelet pools of 5 mice per pool, female). Quantification (right graph) represented as time to 50% aggregation in minutes (min) as median±range; (n=3 platelet pools of 5 mice per pool, female). **(H)** Representative images of laser-induced injury of the cremaster arterioles with stained platelets (green) and fibrin (red) (n=3 male mice per group, 9-10 injuries per mouse, scale bar 10µm). Images taken one and three minutes after injury. **(I)** Dynamics of platelet accumulation and fibrin formation in clots in the cremaster arterioles in *Slc44a2*+/+and *Slc44a2-/-* mice. The kinetic curves represent the mean fluorescence intensity (after subtracting the background) and the shaded regions are representative of the standard error (SEM). Platelets accumulation into the clot (left) and fibrin contents within clot (right) (8-10 independent injury per mouse, 3 mice in each group). Data represents mean±SEM; statistical analysis using 2-way ANOVA. This figure represents data from mice on a FVB background. Figure S1 provides data from mice with a C57BL/6J background corresponding to Figure 1A, B, C, D and I. Data were analyzed with the Instat software (GraphPad, San Diego, USA). Statistical differences between *Slc44a2*+/+and *Slc44a2-/-* were evaluated using a Mann-Whitney Rank sum test unless indicated otherwise. p-values<0.05 were regarded as statistically significant. Abbreviations: Vwf; von Willebrand Factor, Thbd; thrombomodulin, Tfpi; tissue factor pathway inhibitor, Serpine1; serine protease inhibitor E 1, Plat; tissue-type plasminogen activator; Fga; Fibrinogen Alpha Chain, F2; Thrombin, F5; Coagulation Factor V, Proc; Protein C, *Slc44a2*+/+; *Slc44a2* wild-type mice, *Slc44a2-/-*; *Slc44a2* deficient mice.

Acknowledgments

The authors thank Charles Esmon (University of Oklahoma Health Sciences Center, Oklahoma City, OK) for providing 59D8 antibody and Annika de Jong and Richard Dirven for their expertise concerning VWF. Also, we thank the University of Michigan Transgenic core for shipping the transgenic embryos to Leiden. This work was supported by Trombosestichting Nederland (#2015-4), Landsteiner Foundation for Blood Transfusion Research (#1503), travel grant by Boehringer Ingelheim Fonds, NIDCD R01 DC003686, NIGMS R01 GM105671, NHLBI R01 HL114405.

Authorship Contributions

Experimental design: JT, TEC, BJMvV, CXM, MH. Performed experiments and analyzed data: JT, RA, TSN, MEH, DCT, MJ, HMS, CXM. Wrote the paper: JT, BJMvV, CXM. BJMvV supervised the project. All authors commented on manuscript drafts and approved manuscript.

Disclosure of Conflicts of Interest

The authors declare no competing financial interests.

References

1. Day ISCfWT. Thrombosis: a major contributor to the global disease burden. *J Thromb Haemost*. 2014;12(10):1580-90.
2. Germain M, Chasman DI, de Haan H, et al. Meta-analysis of 65,734 individuals identifies TSPAN15 and SLC44A2 as two susceptibility loci for venous thromboembolism. *Am J Hum Genet*. 2015;96(4):532-42.
3. Hinds DA, Buil A, Ziemek D, et al. Genome-wide association analysis of self-reported events in 6135 individuals and 252 827 controls identifies 8 loci associated with thrombosis. *Hum Mol Genet*. 2016;25(9):1867-74.
4. Nair TS, Kozma KE, Hoefling NL, et al. Identification and characterization of choline transporter-like protein 2, an inner ear glycoprotein of 68 and 72 kDa that is the target of antibody-induced hearing loss. *J Neurosci*. 2004;24(7):1772-9.
5. Iwao B, Yara M, Hara N, et al. Functional expression of choline transporter like-protein 1 (CTL1) and CTL2 in human brain microvascular endothelial cells. *Neurochem Int*. 2016;93:40-50.
6. Greinacher A, Wesche J, Hammer E, et al. Characterization of the human neutrophil alloantigen-3a. *Nat Med*. 2010;16(1):45-8.
7. Curtis BR, Cox NJ, Sullivan MJ, et al. The neutrophil alloantigen HNA-3a (5b) is located on choline transporter-like protein 2 and appears to be encoded by an R>Q154 amino acid substitution. *Blood*. 2010;115(10):2073-6.
8. Bayat B, Tjahjono Y, Berghofer H, et al. Choline Transporter-Like Protein-2: New von Willebrand Factor-Binding Partner Involved in Antibody-Mediated Neutrophil Activation and Transfusion-Related Acute Lung Injury. *Arterioscler Thromb Vasc Biol*. 2015;35(7):1616-22.
9. Kommareddi P, Nair T, Kakaraparthi BN, et al. Hair Cell Loss, Spiral Ganglion Degeneration, and Progressive Sensorineural Hearing Loss in Mice with Targeted Deletion of Slc44a2/Ctl2. *J Assoc Res Otolaryngol*. 2015;16(6):695-712.
10. Lakso M, Pichel JG, Gorman JR, et al. Efficient in vivo manipulation of mouse genomic sequences at the zygote stage. *Proc Natl Acad Sci U S A*. 1996;93(12):5860-5.
11. Hemker HC, Giesen P, AlDieri R, et al. The calibrated automated thrombogram (CAT): a universal routine test for hyper- and hypocoagulability. *Pathophysiol Haemost Thromb*. 2002;32(5-6):249-53.
12. Cleuren AC, Van der Linden IK, De Visser YP, et al. 17alpha-Ethinylestradiol rapidly alters transcript levels of murine coagulation genes via estrogen receptor alpha. *J Thromb Haemost*. 2010;8(8):1838-46.
13. Visser YP, Walther FJ, Laghmani el H, et al. Apelin attenuates hyperoxic lung and heart injury in neonatal rats. *Am J Respir Crit Care Med*. 2010;182(10):1239-50.
14. Tjernberg P, Vos HL, Castaman G, et al. Dimerization and multimerization defects of von Willebrand factor due to mutated cysteine residues. *J Thromb Haemost*. 2004;2(2):257-65.
15. Yeung J, Tourdot BE, Adili R, et al. 12(S)-HETrE, a 12-Lipoxygenase Oxylipin of Dihomo-gamma-Linolenic Acid, Inhibits Thrombosis via Galphas Signaling in Platelets. *Arterioscler Thromb Vasc Biol*. 2016;36(10):2068-77.

16. Adili R, Tourdot BE, Mast K, et al. First Selective 12-LOX Inhibitor, ML355, Impairs Thrombus Formation and Vessel Occlusion In Vivo With Minimal Effects on Hemostasis. *Arterioscler Thromb Vasc Biol*. 2017;37(10):1828-39.
17. Adili R, Voigt EM, Bormann JL, et al. In vivo modeling of docosahexaenoic acid and eicosapentaenoic acid-mediated inhibition of both platelet function and accumulation in arterial thrombi. *Platelets*. 2017:1-9.
18. Tourdot BE, Adili R, Isingizwe ZR, et al. 12-HETrE inhibits platelet reactivity and thrombosis in part through the prostacyclin receptor. *Blood Adv*. 2017;1(15):1124-31.
19. Simon LM, Edelstein LC, Nagalla S, et al. Human platelet microRNA-mRNA networks associated with age and gender revealed by integrated plateletomics. *Blood*. 2014;123(16):e37-45.
20. Marx I, Christophe OD, Lenting PJ, et al. Altered thrombus formation in von Willebrand factor-deficient mice expressing von Willebrand factor variants with defective binding to collagen or GPIIbIIIa. *Blood*. 2008;112(3):603-9.

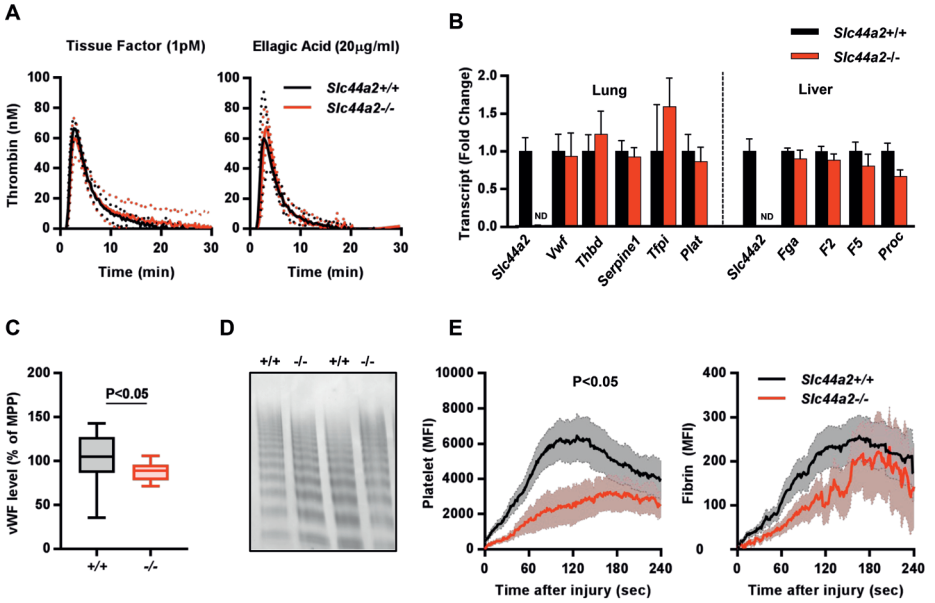

Figure S1. Characterization of hemostasis in Slc44a2 deficient mice on a C57BL/6J (B6) background (A) Thrombin generation in plasma from mice induced either by 1pM Tissue Factor (n=10 for Slc44a2+/+; n=9 for Slc44a2-/-) or 20 µg/mL ellagic acid (n=11 for Slc44a2+/+; n=9 for Slc44a2-/-). Solid lines represent the mean value and dotted lines the standard deviation (SD). (B) Gene transcript levels of Slc44a2 and coagulation related genes in lung and liver (n=15 for Slc44a2+/+; n=11 for Slc44a2-/-). The comparative threshold cycle method with β-actin as internal control was used for quantification and normalization. The mean is represented as fold change compared to Slc44a2+/+ mice. Error bars represent the difference between 2 POWER of upper range of the mean ΔΔCt. ND; non detectable. (C) Levels of plasma vWF expressed as a percentage (%) of (normal) mouse pool plasma (n=14 Slc44a2+/+; n=11 Slc44a2-/-); represented as whisker plot with Tukey. (D) Immunoblot of vWF multimerization in plasma of Slc44a2+/+ and Slc44a2-/- mice (representative of Slc44a2+/+ (n=15) and Slc44a2-/- mice (n=11)). (E) Dynamics of platelet accumulation and fibrin formation in clots in the cremaster arterioles in Slc44a2+/+ and Slc44a2-/- mice. The kinetic curves represent the mean fluorescence intensity (after subtracting the background) and the shaded regions are representative of the standard error (SEM). Platelets accumulation into the clot (left) and fibrin contents within clot (right) (8-10 independent injuries per mouse, 3 mice in each group). Data represents mean±SEM; statistical analysis using 2-way ANOVA. Abbreviations: Vwf; Von Willebrand Factor, Thbd; thrombomodulin, Tfpi; tissue factor pathway inhibitor, Serpine1; serine protease inhibitor E 1, Plat; tissue-type plasminogen activator; Fga; Fibrinogen Alpha, F2; Prothrombin, F5; Coagulation Factor V, Proc; Protein C. *p<0.05.

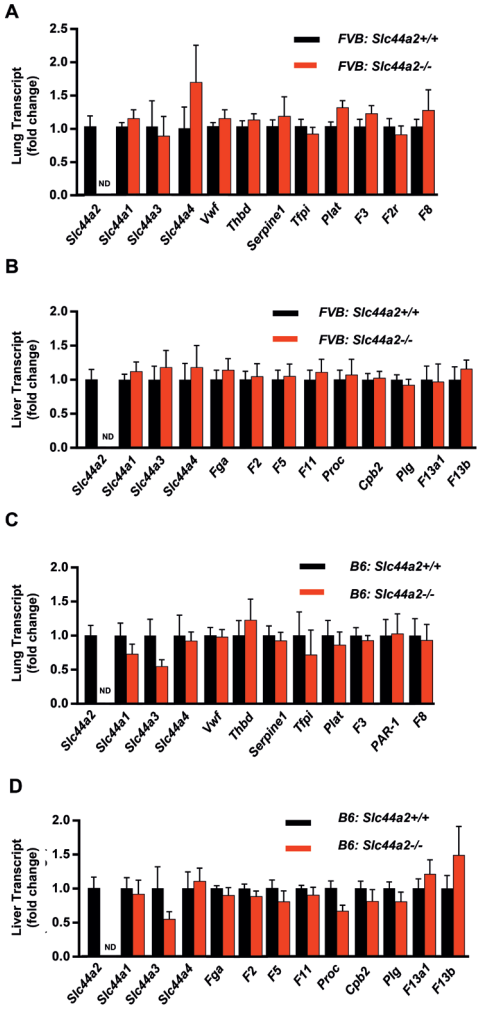

Figure S2. Gene transcript level of *Slc44a* gene family members and coagulation-related genes in liver and lung (A) Lung gene transcript levels in FVB mice (n=11 *Slc44a2*$^{+/+}$; n=7 *Slc44a2*$^{-/-}$). **(B)** Liver gene transcript levels in FVB mice (n=11 *Slc44a2*$^{+/+}$; n=7 *Slc44a2*$^{-/-}$). **(C)** Lung gene transcript levels in B6 mice (n=15 *Slc44a2*$^{+/+}$; n=11 *Slc44a2*$^{-/-}$). **(D)** Liver gene transcript levels in B6 mice (n=15 *Slc44a2*$^{+/+}$; n=11 *Slc44a2*$^{-/-}$). The comparative threshold cycle method with β-actin as internal control was used for quantification and normalization. The mean is represented as fold change compared to *Slc44a2*$^{+/+}$ mice. Error bars represent the difference between 2 POWER of upper range of the mean ΔΔCt. ND; not detectable. Abbreviations: *F3*; tissue factor, *Vwf*; Von Willebrand Factor, *F2r*; coagulation factor II (thrombin) receptor, *F8*; coagulation factor VIII, *Thbd*; thrombomodulin, *Tfpi*; tissue factor pathway inhibitor, *Serpine1*; serine protease inhibitor E 1, *Plat*; tissue-type plasminogen activator, *Fga*; Fibrinogen Alpha , *F2*; Prothrombin, *F5*; Coagulation Factor V, *F11*; Coagulation Factor XI, *Proc*; Protein C, *Cpb2*; thrombin-activatable fibrinolysis inhibitor, *Plg*; Plasminogen, *F13a1*: coagulation factor XIIIa, *F13b*: coagulation factor FXIIIb.

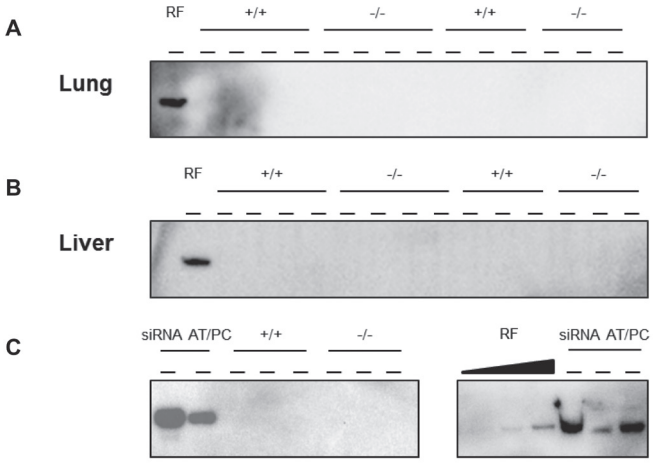

Figure S3. Fibrin deposition in lung and liver. Immunoblot for fibrin in FVB;*Slc44a2*$^{+/+}$ (+/+) and FVB;*Slc44a2*$^{-/-}$ (-/-) mouse lung (A) and liver (B). Each lane represents tissue from 1 mouse per genotype (n=7). RF: positive control; purified rat fibrinogen converted fibrin and processed for immunoblot identical to mouse tissue samples. (C) Immunoblot with additional fibrin positive liver control samples from C57BL/6J mice injected with siRNA targeting *Serpinc1* and *Proc* (siRNA AT/PC) (N=2). These mice were previously established to exhibit fibrin deposition (Safdar et al. Blood 2013) (left panel). Immunoblot with the two positive controls: fibrin converted from rat fibrinogen, that is used throughout the procedure for calibration, and material from mice treated with siRNA AT/PC (right panel). Results for liver and lung of B6;*Slc44a2*$^{+/+}$ and B6;*Slc44a2*$^{-/-}$ animals are comparable (no fibrin detectable, not shown).

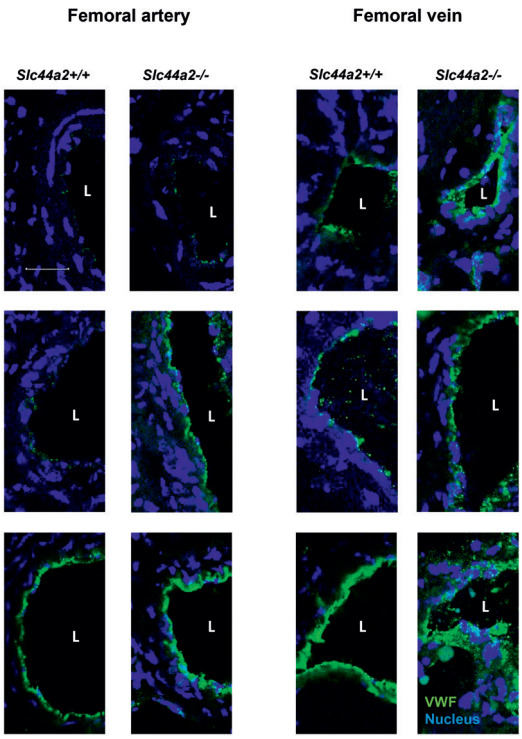

Figure S4. Confocal microscopic images of VWF in the femoral vein and artery. Von Willebrand Factor (green) staining of the femoral artery (left panels) and vein (right panels) from FVB,*Slc44a2*$^{+/+}$ and FVB,*Slc44a2*$^{-/-}$ mice. L; Lumen. (Representative images for 5 mice per genotype that have low, moderate or abundant signal for VWF immunostain. Note: Images shown for each mouse represent one out of the 8 to 9 stacks available per imaged section; Scale bar 30μM). VWF; Von Willebrand Factor.

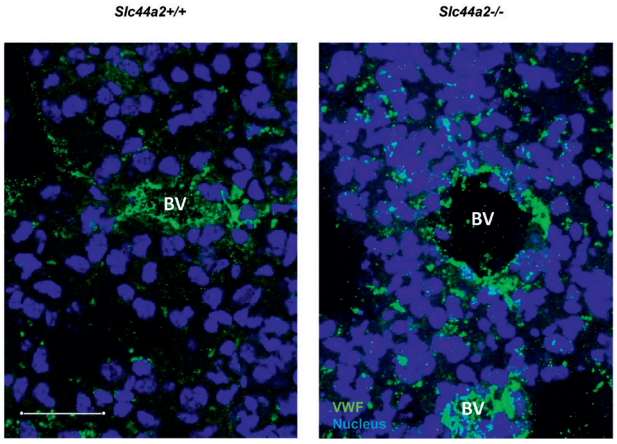

Figure S5. Confocal microscopy images of VWF in microvasculature of the lung. Von Willebrand Factor (green) staining of lung tissue from FVB,*Slc44a2*$^{+/+}$ and FVB,*Slc44a2*$^{-/-}$ mice. Lungs were snap frozen in liquid nitrogen making the architecture of the lung alveolar no longer clearly visible, BV; blood vessel. (Representative images for 5 mice per genotype. Note, Images shown for each mouse represents one out of the 8 to 9 stacks available per imaged section; Scale bar 30µM). VWF; Von Willebrand Factor.

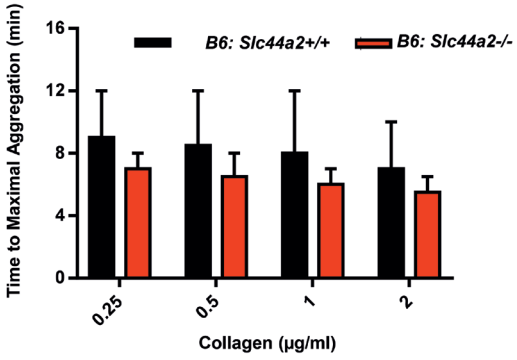

Figure S6. Ex-vivo platelet aggregation Collagen induced platelet aggregation using pooled platelets from *Slc44a2*$^{+/+}$ and *Slc44a2*$^{-/-}$ mice with different concentrations of collagen, represented as time in minutes (min) to maximal aggregation as median±range; (n=2 platelet pools of 5 mice per pool, female).

Table S1 qPCR primer sequences used for (coagulation) gene profiling of lung and liver

Gene	Forward primer	Reverse primer
Actb Reference	AGGTCATCACTATTGGCAACGA	CCAAGAAGGAAGGCTGGAAAA
Slc44a1	ACCCACCGGAAGTATGTGTTC	GCTGCTACGCACAGTGCTA
Slc44a2	CGGAAGGACGCAGTCTATGG	AGGAAGAGCAACACACAGCA
Slc44a3	ATGAATGCCTGCAATCTTGAAGT	GACCTCTTCCAGAGTGTCCAG
Slc44a4	AGAATGAGAACGAGGCTCACG	CCCCACTATGATGTAACCCAAAA
Slc44a5	ATGATGCTCCGGCTACAGTG	TCCAAGTAGGTGAGGAATCTCTC
F3	ACCAAAATAGCCCAGGAAGC	CCAGGAAACTCTTCCATTGC
Vwf	AGCTGTCAGCCAGGTTTTTCTT	GCAGAGGGCAGGCACCTT
F2r	TGCTGGGAGGTATCACCCTTC	GCTGGGTTTCTAATCTGCCAAT
F8	CTTCACCTCCAGGGAAGGACTA	TCCACTTGCAACCATTGTTTTG
Thbd	CACAGGCAGTCAATGCGTG	GAGCGCACTGTCATCAAATGT
Tfpi	GGCTTCGCCTTTCAGAGTG	GAGAACGACCTCATACGTTGTAG
Serpine1	CCCTGGCCGACTTCACAA	TTTTGCAGTGCCTGTGCTACA
Plat	AGATGAGCCAACGCAGACAA	AACTTCGGACAGGCACTGAG
Fga	TGCTGCCTGCTTTTACTGTTCTC	TCTAGGATGCAACAGTTATCTCTGGTA
F2	GGACGCTGAGAAGGGTATCG	CCCCACACAGCAGCTCTTG
F5	CATGGAAACCTTACCGACAGAAA	CATGTGCCCCTTGGTATTGC
F11	GAAGGATACGTGCAAGGGAGATT	CAAGTGCCAGACCCCATTGT
Proc	GCGTGGAGGGCACCAA	CCCTGCGTCGCAGATCAT
Cpb2	GGCTTCGCCTTTCAGAGTG	GAGAACGACCTCATACGTTGTAG
Plg	GGAGGTGTCTCGGACTGTTTG	GATGCCGGTCTTACATTCTGAC

Table S2 Blood cell counts and *Slc44a2* status

FVB*	*Slc44a2*+/+ Median [range]	*Slc44a2*-/- Median [range]
Platelets (K/μL)	745 [441-904]	455 [241-677]
Erythrocytes (K/μL)	8.62 [7.62-10.49]	8.53 [7.08-10.74]
White Blood Cells (K/μL)	8.92 [6.26-14.04]	10.99 [6.26-12.4]
B6[#]	*Slc44a2*+/+ Median [range]	*Slc44a2*-/- Median [range]
Platelets (K/μL)	601 [466-856]	626 [328-972]
Erythrocytes (K/μL)	8.00 [6.94-8.70]	7.96 [3.48-8.58]
White Blood Cells (K/μL)	5.2 [3.4-11.0]	4.6 [2.4-6.8]

*Analyzed using Hemavet950FS (N=5), analysis only performed for mice used in platelet aggregation experiments (Figure 1G).

[#]Analyzed using SysmexXT-2000iV (N=12).